



Photocatalytic hydrogen production on Pt-loaded TiO₂ inverse opals

Fabrizio Sordello*, Claudio Minero*

Dipartimento di Chimica, Università di Torino, Via P. Giuria, 5, 10125 Torino, Italy

ARTICLE INFO

Article history:

Received 22 May 2014

Received in revised form 1 August 2014

Accepted 19 August 2014

Available online 24 August 2014

Keywords:

TiO₂

Inverse opal

Hydrogen production

Slow light

Slow photons

ABSTRACT

TiO₂ inverse opals present increased photocatalytic production of H₂. TiO₂ inverse opals with different pore size and TiO₂ macroporous structures with disordered arrangement of the pores have been tested in the photocatalytic production of hydrogen in aqueous solution with a formate buffer as hole scavenger. TiO₂ inverse opals belong to the family of metamaterials and exhibit unique catalytic properties arising from their peculiar interaction with light. To discriminate the effects of slow photons the hydrogen photoproduction experiments were carried out at two different wavelengths, at 365 nm where the effect of slow photons is maximized, and at 254 nm where it is negligible. The resulting hydrogen production rates suggest a strong effect of the slow light and of the polymer template used in the synthesis of the TiO₂ powders. The chemical properties of the polymeric sacrificial template determine the crystalline phase of the sample and as a consequence affect the catalytic performances of the resulting TiO₂ structures.

© 2014 Elsevier B.V. All rights reserved.

1. Introduction

Photonic crystals are materials in which the refractive index varies periodically in the space, and, since light can be refracted and reflected at each interface, for a wavelength matching the lattice periodicity there is the possibility to have constructive interference of the reflected waves. At that wavelength light is completely reflected and cannot propagate inside the material because of the presence of the photonic band gap (PBG) [1,2]. Owing to this, photonic crystals find applications as dielectric mirrors [3–6], waveguides [7], lasing cavities [8,9], and black body radiation modifiers [10]. At the PBG edges light can propagate inside the photonic crystal, but its group velocity is strongly reduced, and thus its interaction with the material increases, opening the field to a series of diversified applications [11,12].

The increased light-matter interaction can be exploited in photocatalysis. Recently Tsai et al. published an interesting report [13] on the interaction of light with hierarchical structured TiO₂, specifically hollow spheres, which could harvest more light thanks to the scattering effect in the microstructure while maintaining high surface area. Among photonic crystals TiO₂ inverse opals (TIOs) have been studied extensively to improve the efficiency of

the photocatalytic process [14–16]. TIOs are constituted of ordered arrays of holes in a TiO₂ matrix, but they only possess a partial PBG, because the refractive index of TiO₂ is not high enough to open an omnidirectional gap [17]. Previous results show that TIOs can significantly increment the photocatalytic performances of TiO₂ thanks to the slow light phenomenon, which is the improved light-matter interaction due to the reduction of the group velocity of light at the PBG edges [18–21]. In a previous work [21] we have clarified that besides slow photons, porosity and specific surface area give only a negligible contribute to the observed increase in photocatalytic activity of these structures. The photoelectrochemical study of such materials [22] showed that TIOs and disordered macroporous TiO₂ structures share the same recombination rate of the photogenerated charge carriers, but TIOs are characterized by a faster electron transfer to the oxygen present in solution. After our early analysis, other research works observed that the slow photon effect markedly improved the photocatalytic activity in the oxidation of dyes [23], and increased three times the performance of Bi₂WO₆ deposited on SiO₂ photonic crystal compared to ordinary Bi₂WO₆ films [24]. The slow photon effect was also responsible for the enhanced photodegradation of the AO7 dye on TIOs doped with Ti³⁺ [25]. Conversely, the porous structure plays an important role in electrocatalytic reactions [26]. Thus the enhanced absorption of light, the improved reactivity towards oxygen and, to a lesser extent, the improved mass transfer of substrates make TIOs good candidates as catalysts for photo-reduction reactions.

To test the presence of a synergic effect between slow light and faster electron transfer to solution, in the present work we have compared the activity of Pt-loaded TIOs and of Pt-loaded

Abbreviations: PBG, photonic band gap; TIO, TiO₂ inverse opal; MP, macroporous; XRD, X-ray diffraction; PMMA, polymethylmethacrylate; PS, polystyrene.

* Corresponding authors. Tel.: +39 011 670 5294/8449; fax: +39 011 670 5242.

E-mail addresses: fabrizio.sordello@unito.it, fabrizio.sordello@gmail.com (F. Sordello), claudio.minero@unito.it (C. Minero).

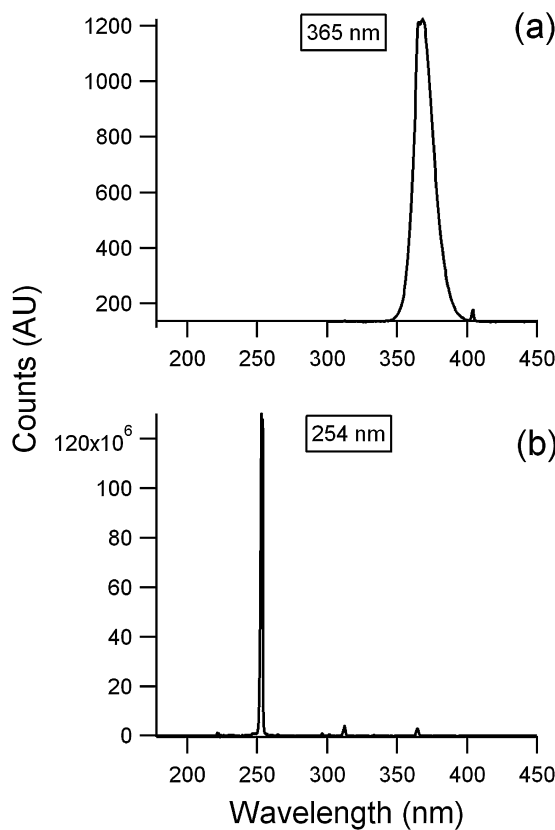


Fig. 1. Emission spectra of a Philips TUV PL-S lamp (a) and of a Philips PLS-10 lamp (b).

macroporous disordered TiO_2 structures in hydrogen photoproduction experiments. To detect the effect of slow photons we performed irradiations at two different wavelengths: at 365 nm, where the TiO_2 s synthesized can take advantage of slow light, and at 254 nm, where for the TiO_2 s considered the slow light contribution to the photocatalytic activity is negligible. The hydrogen production rates of TiO samples are then compared with those of disordered macroporous samples.

2. Experimental

2.1. General

TiO_2 P25 was a gift of Degussa, methyl methacrylate (MMA, 99%), styrene (99%), 2,2'-azobis(2-methylpropionamidine) dihydrochloride (97%), titanium (IV) isopropoxide (97%), hexachloroplatinic acid hexahydrate (37.5% Pt basis), formic acid (85% in water), ethanol (99.9%) and ethylene dimethacrylate (98%), were purchased from Aldrich, sodium formate (99%) from Merck. All the products were used without further purification.

2.2. Powder preparation

TiO_2 and TiO_2 macroporous structures were synthesized using different polymeric sacrificial templates. Polymethylmethacrylate (PMMA) and polystyrene (PS) templates were used to obtain TiO_2 structures with different pore sizes. The detailed synthesis procedure has been described elsewhere [21], here we only summarize the relevant issues. PMMA syntheses were carried out following a modified method proposed by Waterhouse and Waterland [27], in which the stirring procedure was changed [21]. With vigorous mechanical stirring well monodisperse colloids were

Table 1
Specific surface area, diameter of the macropores and TiO_2 crystalline phases present in the TiO_2 powders synthesized (A: anatase, B: brookite, R: rutile).

Sample	SSA ($\text{m}^2 \text{g}^{-1}$)	Macropore size (nm)	Crystalline phases
TIO-PMMA	18	125	Anatase, rutile < 1%
MP-PMMA	28	200–220	Anatase, rutile \approx 2%
TIO-PS	74	330	A \approx 57%, B \approx 36%, R \approx 7%
MP-PS	69	300–330	A \approx 70%, R \approx 30%
P25	45 [46]	–	A \approx 80%, R \approx 20% [47]

produced, whereas with magnetic stirring polydisperse colloids were obtained.

Monodisperse polystyrene (PS) spheres were prepared with emulsion polymerization without emulsifier with a modified version of the method proposed by Goodwin et al. [28]. The size of the PS spheres produced is highly dependent on the composition of the synthesis mixture and on the reaction temperature, while the monodispersity of nanoparticles strongly depends on the stirring of the reaction mixture. To obtain well monodisperse colloids we carried out syntheses with mechanical stirring. Polystyrene polydisperse colloids were obtained mixing various batches of monodisperse colloids.

Polymer colloid size and polydispersity were measured with an ALV-NIBS High Performance Particle Sizer (ALV GmbH). Polymeric colloidal suspensions were diluted approximately from 5 to 100-fold with Milli Q water before measurements and the particle size was extrapolated at infinite dilution.

Opals made with monodisperse polymer particles and polymeric disordered structures have been prepared loading PMMA or PS colloidal suspensions into 50 mL plastic falcon tubes followed by centrifugation (4300 rpm, 15 °C for 90 min). The supernatant was then removed, and the polymeric disordered structure or the polymeric colloidal crystal was left to dry in air at 25 °C for 24 h.

Macroporous TiO_2 (MP) and TIOs were prepared filling the interstices among polymer spheres in polymeric disordered structures and polymeric opals with a TiO_2 precursor. 1.5 g of the polymer template were gently crushed with a metal spatula to give fractured pieces of size <2 mm, which were then deposited on a filter paper (Whatman, Qualitative 1, 11 µm) placed into a sintered glass filter funnel (Millipore). With a strong vacuum applied to the sintered glass filter funnel, a solution of TiO_2 precursor (4 mL titanium (IV) isopropoxide and 4 mL ethanol) was poured drop wise over the surface of the polymeric structure. Infiltrated samples were then left to dry in air at 25 °C for 2 h and recovered. Polymeric templates were then removed by means of calcination in air using the following protocol: the temperature was raised from 25 to 300 °C at 2 °C min⁻¹, held at 300 °C for 5 h, then raised again from 300 to 550 °C at 2 °C min⁻¹, held at 550 °C for 12 h. Samples were then finally allowed to cool to room temperature over 3–4 h.

On the as prepared materials, Pt was photocatalytically reduced adding H_2PtCl_6 to catalyst slurries and irradiating with UV light (see below).

2.3. X-ray powder diffraction

X-ray powder diffraction (XRD) patterns have been recorded with a PW3050/60 X'Pert PRO MPD diffractometer from PANalytical working in Bragg-Brentano configuration. The X-ray source was a high power ceramic tube PW3373/10 LFF with a Cu anode and the instrument was equipped with a Ni filter to attenuate K_β . Diffracted photons were collected with a real time multiple strip X'celerator detector. Powder samples have been hosted on SiO_2 amorphous sample holder.

The relative amounts of the different TiO_2 polymorphs were assessed with the method proposed by Zhang and Banfield [29].

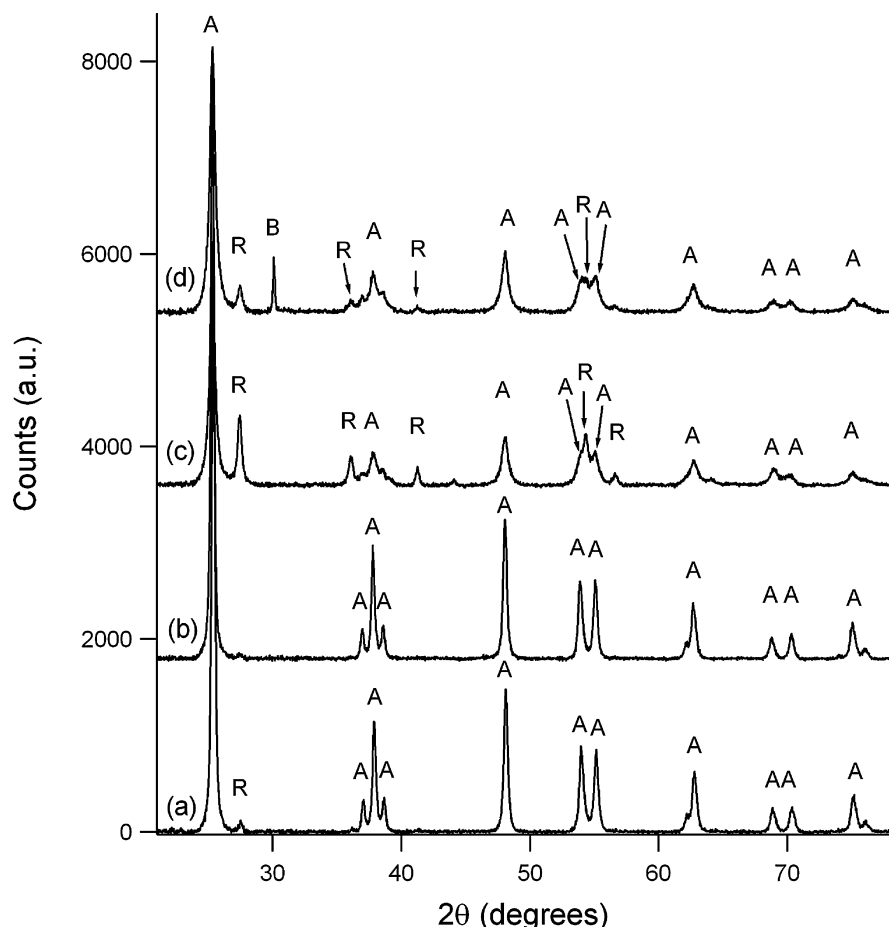


Fig. 2. XRD patterns of (a) MP-PMMA, (b) TIO-PMMA, (c) MP-PS and (d) TIO-PS. The letter A denotes anatase, B denotes brookite and R denotes rutile.

2.4. Specific surface area

The specific surface area (SSA) of the powders synthesized was measured with nitrogen adsorption using an ASAP 2010 instrument (Micromeritics Instrument Corporation). Before the analysis all the samples were outgassed at 300°C in vacuum for 24 h. Specific surface area was calculated with the B.E.T. method [30], assuming an area of 0.162 nm^2 for the N_2 adsorbed molecule.

2.5. Hydrogen production

The hydrogen production experiments were carried out irradiating with UV light slurries containing 1 g L^{-1} of TiO_2 powder and 2 mg L^{-1} of Pt, added as H_2PtCl_6 . The pH of the suspension was buffered at 3.8 with the addition of a formic acid–sodium formate buffer 0.1 M. The formate buffer acts also as hole scavenger. The irradiation experiments were carried out in magnetically stirred, cylindrical quartz cells (3.5 cm inner diameter, 2 cm height), containing 5 mL of slurry. Before irradiation the cell containing the slurry was carefully purged with nitrogen to remove oxygen from the reaction environment. Hydrogen evolution was followed withdrawing periodically 2.5 ml of gas from the irradiation cell and replacing it with the same volume of N_2 . The gas sample was analyzed with an Agilent 490 Micro GC gas chromatograph equipped with a Molsieve 5 \AA column. During the analysis the column was kept at a temperature of 90°C and at a pressure of 200 kPa, the carrier gas was argon. The total amount of H_2 produced as a function of time was calculated from the concentration in the sampled gas,

from the volume of gas in the irradiation cell and considering the previous samplings.

To evaluate the effect of the slow photons the irradiations were performed at two different UV wavelengths (365 nm and 254 nm). The radiation source at 365 nm was a Philips PLS-10 lamp at a distance of 10 cm from the quartz cell with a flat Al foil as a reflector. The irradiance on top of the solutions was 78 W m^{-2} , measured with a CO.FO.ME.GRA. power metre. Irradiation at 254 nm was carried out with a 9W Philips TUV PL-S lamp at a distance of 10 cm from the quartz cell, emitting 2.3 W in UVC. Fig. 1 reports the emission spectra of the two lamps, measured with an Ocean Optics SD2000 CCD.

2.6. Computational details

Photonic bands diagrams have been calculated with a freely available software [31].

3. Results and discussion

3.1. Powder characterization

In the present work five different samples have been studied. Among them two have been prepared starting from PMMA templates. Their AFM, SEM and optical spectra, as well as the photocatalytic activity towards phenol oxidation have been investigated in a previous work [21]. Two samples have been obtained from PS templates, and, besides the optical and morphological characterization, on them an extensive photoelectrochemical study has been

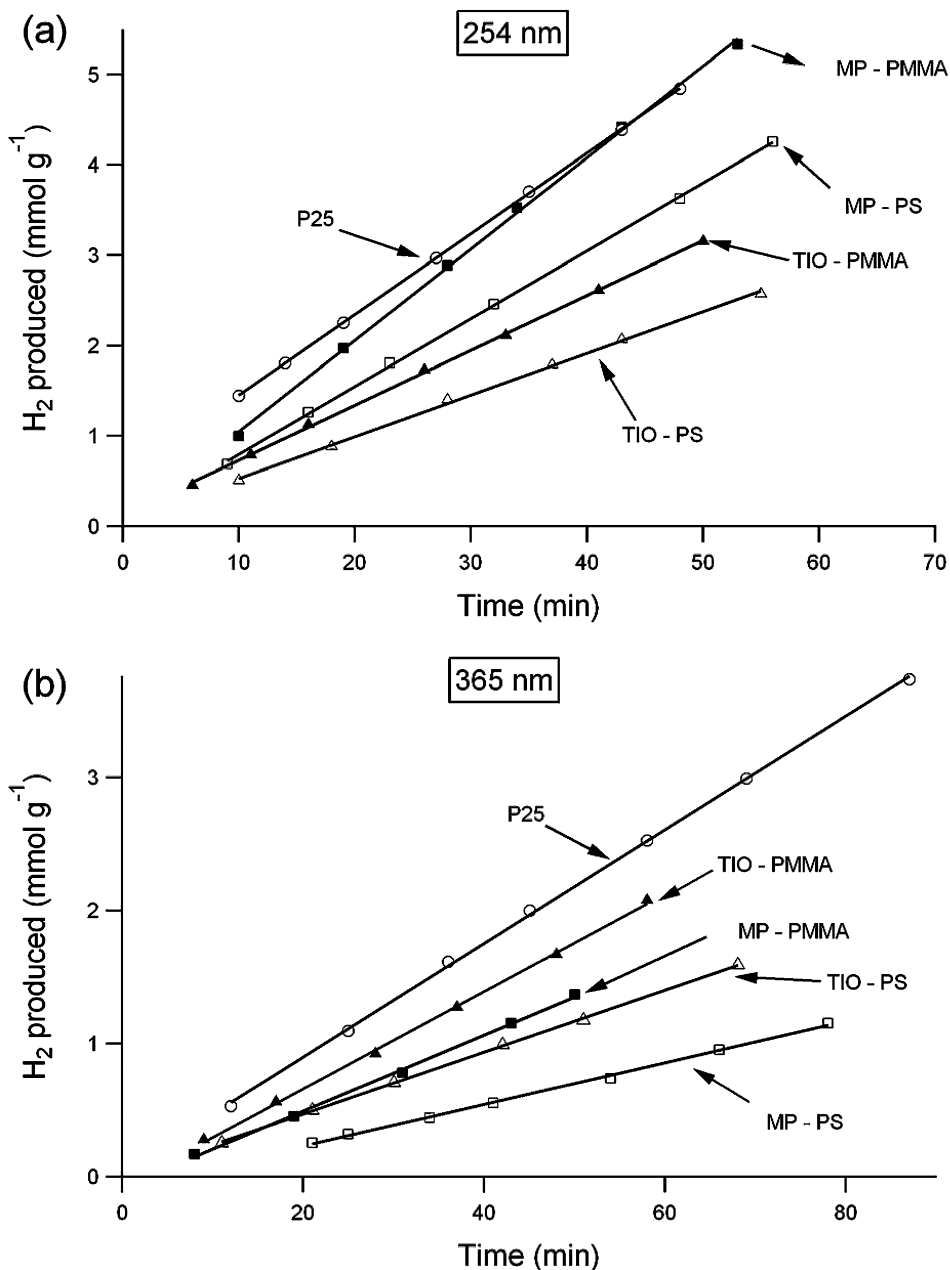


Fig. 3. Hydrogen produced as a function of the irradiation time for suspensions containing 1 g L^{-1} of different TiO_2 powders and 2 mg L^{-1} of Pt in the presence of formate buffer 0.1 M at pH 3.8. The radiation source had an emission maximum at 254 nm (a) and at 365 nm (b).

performed by means of voltammetry, potentiometry and electrochemical impedance spectroscopy [22]; the fifth sample was P25, here used as a reference for the activity of the synthesized samples.

The sample prepared using PMMA disordered structure as a template (macroporous disordered structure, MP-PMMA) is a macroporous powder with disordered pore structure, and as a consequence there is no PBG. Using PMMA ordered structure as a template, the inverse opal was obtained (TIO-PMMA). The inverse opal TIO-PMMA has a pore structure with long range order. During calcination the PMMA template shrinks considerably (up to 50%). Starting from PMMA with particle diameter about 250 nm, the sample TIO-PMMA has pores with diameter around 125 nm (pseudo-PBG around 280 nm in air, 320–330 nm in water). Starting from PMMA with particle diameter around 420–450 nm, the sample MP-PMMA has pores with a mean diameter around 220 nm [21].

The TIO-PS sample, prepared from the PS opal powder, has an ordered arrangement of the pores, each pore has a diameter of 250 nm and it is separated from its closest neighbours by 80 nm thick TiO_2 walls. The corresponding opal template was composed of PS spheres with diameter of 360 nm, indicating a limited shrinkage with respect to PMMA. In this case the pseudo-PBG is located at 500 nm, but there are photonic bands characterized by low group velocity also at 330–380 nm [22]. The sample MP-PS has a very similar pore size distribution, but its structure lacks in long range order, and, as in the case of MP-PMMA, there is no PBG and no way to exploit the slow photon effect [22].

The pore size distributions and the specific surface areas (SSA) of the samples synthesized are summarized in Table 1. The powders obtained from PS templates have higher specific surface area with respect to PMMA templates. In addition the data of Table 1 suggest that the surface area increases with the pore size at the $3/2$ power,

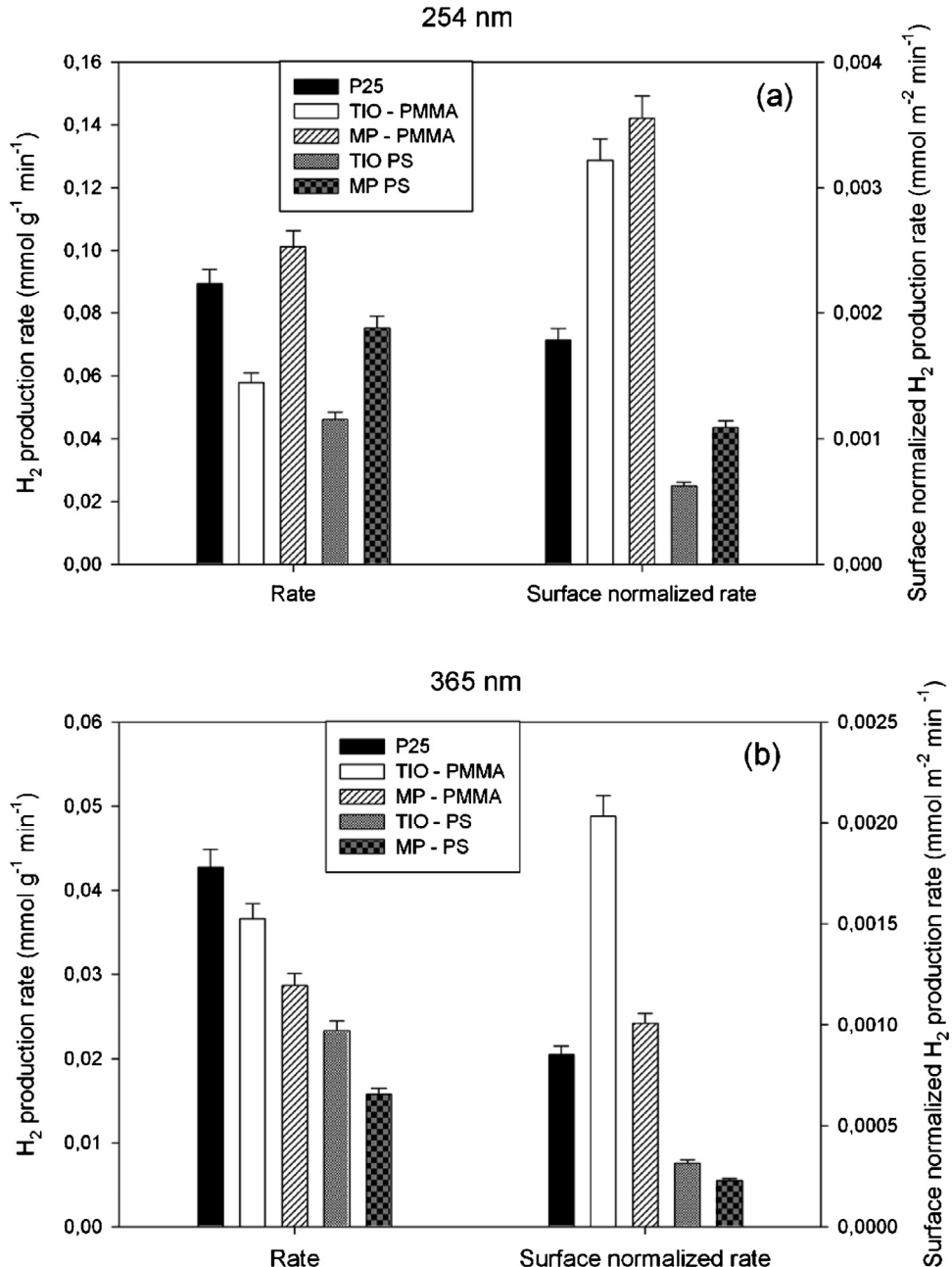


Fig. 4. Hydrogen production rates and surface normalized rates for powder samples irradiated at 254 nm (a) and at 365 nm (b). All samples were suspensions containing 1 g L^{-1} of different TiO_2 and 2 mg L^{-1} of Pt in the presence of formate buffer 0.1 M at pH 3.8.

opposite to the expected inverse dependence. As mentioned before PMMA templates shrink during calcination, and this process can cause the occlusion of part of the macropores, resulting in a reduced SSA. In the case of smaller macropores the channels connecting the macropores network are also smaller and easier to occlude.

X-ray powder diffractograms reported in Fig. 2 show that anatase is the dominant TiO_2 crystalline phase when PMMA is used as sacrificial template, while rutile is present only as a trace (<2%). When PS is used as polymer template, the presence of rutile and brookite, in the sample TIO-PS, becomes significant. MP-PS contains about 30% of rutile, while TIO-PS is composed of 57% anatase, 36% brookite and 7% rutile. These relative amounts are only approximate, because it is not possible to finely homogenize the samples without losing the properties arising from the 3D structure of the powders. These differences in compositions can

be explained in terms of the chemical properties of the polymer templates. PMMA has a certain number of carboxylate groups, and it is known that carboxylate can complex preferentially anatase $\{001\}$ facets, changing the growing rate ratio of $\{001\}$ facets to $\{101\}$ facets [32–35]. The diffractograms reported in Fig. 2 suggest also that the carboxylate groups can favour the nucleation of anatase rather than rutile or brookite, since in the samples obtained using PMMA as template rutile and brookite are almost absent.

3.2. Hydrogen production

The initial slurry contains the photocatalyst as a suspended solid, H_2PtCl_6 and the formate buffer. In the first step of the irradiation, the photoelectrons produced by UV light reduce Pt(IV) to Pt(0) , and are responsible for the Pt photodeposition [36]. In

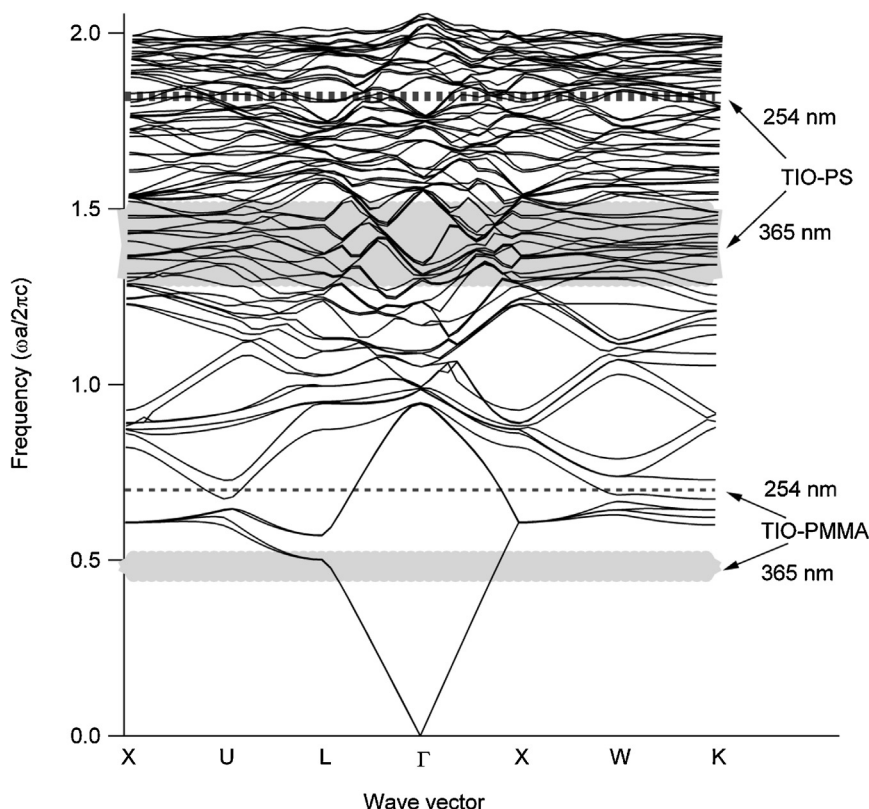


Fig. 5. Calculated photonic band diagram for TiO₂ powders in water with data of Table 1. The frequencies used during irradiation experiments are highlighted. For TiO₂ $\varepsilon_1 = 5.5$; for water $\varepsilon_1 = 1.7$.

this process the formate buffer has the function of hole scavenger. Once the Pt is deposited and the suspension turned to a pale grey, the production of hydrogen started. Fig. 3 reports the cumulative hydrogen produced as a function of the time. The extrapolation of the trends when hydrogen production starts (intercept with the abscissa) shows that at both 254 nm and 365 nm the hydrogen evolution begins even before the fifth minute of irradiation. In some cases the hydrogen evolution seems to start at even negative times: this effect is due to the non-linearity of hydrogen production in the very first minutes of irradiation, after which it follows a linear trend. The rates are reported in Fig. 4, together with the rates normalized by the SSA.

From a general analysis of the plots in Figs. 3 and 4 it can be seen that at 254 nm the hydrogen production rates and the SSA normalized rates roughly double with respect to the rates observed at 365 nm. The comparison of the absolute rates at 254 nm and 365 nm is challenging because the intensity of the incident light is different, and other factors like the different absorption coefficient of TiO₂ at those wavelengths and the different scattering of light [37] are difficult to be estimated. Thus, only are the relative rates at each wavelength significant to assess the role of the material geometrical arrangement.

Considering the 365 nm irradiation using the TIO-PMMA and MP-PMMA samples (Fig. 4b) it can be seen that the ordered three dimensional structure nearly doubles the surface normalized photocatalytic activity of P25 and macroporous disordered specimen. The same observation can be made for the powders obtained from PS templates, even if, in this case, TIO-PS is only 25% more active than its macroporous homologue (Fig. 4b). In general, both for the rate and the normalized rate the performance is in the order MP < TIO. Since at those photon energies flat photonic bands in the diagram frequency (ω) vs wavevector (k) are present for both

TIO-PMMA and TIO-PS (Fig. 5), slow photons can reasonably be the cause of the observed differences in hydrogen production, since, considering separately PMMA and PS derived samples, minor differences in surface chemistry or crystallinity exist due to the same synthesis conditions. Thus, the major difference among TIO₂s and their macroporous MP analogues is the 3D arrangement of the pores that influences the ability to absorb the incident light.

At 254 nm (Fig. 4a), both for the rate and the normalized rate the performance follows the trend MP > TIO. The surface normalized rate of the sample TIO-PMMA is very similar to that of MP-PMMA, and in the case of PS template samples MP-PS is definitely more active than TIO-PS. Considering the photonic band diagram of TIO-PS (Fig. 5) at 254 nm there are few photonic bands characterized by a low group velocity. At those energies TiO₂ has a higher absorption coefficient [38], and the lengthening of the effective optical path due to slow photons is not crucial in increasing the absorbance.

Comparing now the rates of the samples focusing on the different chemical composition of the templates (Fig. 4) it can be noticed that although the rates are comparable, the surface normalized rates of PS samples are significantly lower with respect to PMMA samples both at 365 nm and 254 nm, because of the higher SSAs of the PS samples. The polymer template has an influence on the crystalline phases present in the synthesized samples (Fig. 2) and also an effect on the surface properties is very likely. Since photocatalytic properties depend on the TiO₂ crystalline phases and on the surface exposed [39], the choice of the polymer template has an influence on the behaviour of the material under irradiation. It has been demonstrated that the activity in hydrogen photoproduction depends on the particle shape and on the facets exposed by the catalyst, and anatase nanoparticles synthesized in the presence of carboxylic acids and exposing {001} facets are very active [40,41]. The fact that TiO₂ structures obtained from PMMA templates are,

for the most part, more active than those obtained with PS is in agreement with those results. Moreover, the presence of rutile in the PS samples, characterized by a lower energy of the conduction band [42] with respect to anatase, decreases the energy of the conduction band with respect to samples obtained from PMMA, where almost only anatase is present (Table 1), and decreases the overpotential available for the H₂ production, resulting in a lower activity.

We reported a higher reaction rate of photogenerated electrons with oxygen present in solution for the TiO-PS sample with respect to its MP-PS homologue, while the recombination rate of the photo-generated charge carriers was the same in both TiO-PS and MP-PS [22]. Following this evidence, we expected a faster hydrogen evolution from the TiO-PS sample by irradiation at 254 nm, where the effect of slow photons is negligible. A greater activity of TiOs at 254 nm would be the evidence of a faster electron transfer rate in TiOs with respect to macroporous analogues. On the contrary, we observed slightly lower activities for the TiOs compared to MP samples (Fig. 4a). This is the evidence that the improvement in TiO activity at 365 nm is entirely due to the slow photon effect (Fig. 4b). This also suggests that the electron transfer to solution via the Pt co-catalyst on TiOs is by no means faster than for MP structures. The production of H₂ occurs on Pt sites with small overpotentials, and the rate determining step can be the electron transfer from the metal to H⁺ or water [43], or the catalytic desorption of H₂ from the Pt surface [44]. This situation is completely different from the dioxygen reduction on TiO₂, where the reduction occurs on adsorbed oxygen (surface traps) with high overpotentials [43].

4. Conclusions

Irradiation experiments performed at 254 nm show that TiOs and disordered MP structures obtained from the same polymer template (PMMA or PS) have hydrogen production rates in the order MP > TiO. Upon irradiation at 365 nm due to the slow light phenomenon the synthesized TiO₂ inverse opals have hydrogen production rates (or SSA normalized rates) larger than disordered macroporous structures that did not possess an ordered arrangement of the pores (MP < TiO). The increase in activity is due to a better exploitation of the incident light. The rate of the synthesized TiO₂ powders is also influenced by the chemical properties of the polymeric template, which determines not only the pore size and the order of the pore structure, but also the TiO₂ crystalline phases. Nevertheless, these and other factors such as the kinetics of the charge transfer at the interface, or the different crystalline facets exposed [45], cannot account for the different orders of reactivity found at different irradiation wavelengths, because the improved absorption of light is the cause of this phenomenon, which is observed both for oxidation [20] and, in this work, for reduction reactions. Owing to this, the strategy can be conveniently used in every photocatalytic reaction.

Acknowledgements

The authors thank Dr. Giuliana Magnacca for her helpfulness and expertise in nitrogen adsorption experiments. The financial support from project PHOTORECARB – Progetti di Ateneo/CSP 2012 – Call 03 – Università di Torino & Compagnia di S.Paolo – is gratefully acknowledged.

References

- [1] E. Yablonovitch, *Sci. Am.* 285 (2001) 46–50.
- [2] J.D. Joannopoulos, S.G. Johnson, J.N. Winn, R.D. Meade, *Photonic Crystals Mold-ing the Flow of Light*, second ed., Princeton University Press, Princeton, 2008.
- [3] M. Ishii, M. Harada, A. Tsukigase, H. Nakamura, *J. Opt. A-Pure Appl. Op.* 9 (2007) S372–S376.
- [4] A. Mihi, M.E. Calvo, J.A. Anta, H. Miguez, *J. Phys. Chem. C* 112 (2008) 13–17.
- [5] S. Nishimura, N. Abrams, B.A. Lewis, L.I. Halaoui, T.E. Mallouk, K.D. Benkstein, J. van de Lagemaat, A.J. Frank, *J. Am. Chem. Soc.* 125 (2003) 6306–6310.
- [6] P.G. O'Brien, N.P. Kherani, A. Chutinan, G.A. Ozin, S. John, S. Zukotynski, *Adv. Mater.* 20 (2008) 1577–1582.
- [7] X. Letartre, C. Seassal, C. Grillet, P. Rojo-Romeo, P. Viktorovitch, M.L. d'Yerville, D. Cassagne, C. Jouanin, *Appl. Phys. Lett.* 79 (2001) 2312–2314.
- [8] I.D.W. Samuel, G.A. Turnbull, *Chem. Rev.* 107 (2007) 1272–1295.
- [9] A. Mekis, M. Meier, A. Dodabalapur, R.E. Slusher, J.D. Joannopoulos, *Appl. Phys. A: Mater. Sci. Process.* 69 (1999) 111–114.
- [10] M. Florescu, H. Lee, I. Puscasu, M. Pralle, L. Florescu, D.Z. Ting, J.P. Dowling, *Sol. Energy Mater. Sol. Cells* 91 (2007) 1599–1610.
- [11] T. Baba, *Nat. Photonics* 2 (2008) 465–473.
- [12] Y. Zhao, H.-W. Zhao, X.-Y. Zhang, B. Yuan, S. Zhang, *Opt. Laser Technol.* 41 (2009) 517–525.
- [13] M.-C. Tsai, J.-Y. Lee, P.-C. Chen, Y.-W. Chang, Y.-C. Chang, M.-H. Yang, H.-T. Chiu, I.N. Lin, R.-K. Lee, C.-Y. Lee, *Appl. Catal. B: Environ.* 147 (2014) 499–507.
- [14] M.M. Ren, R. Ravikrishna, K.T. Valsaraj, *Environ. Sci. Technol.* 40 (2006) 7029–7033.
- [15] M. Srinivasan, T. White, *Environ. Sci. Technol.* 41 (2007) 4405–4409.
- [16] Q. Li, J.K. Shang, *J. Am. Ceram. Soc.* 91 (2008) 660–663.
- [17] W.T. Dong, H.J. Bongard, F. Marlow, *Chem. Mater.* 15 (2003) 568–574.
- [18] F. Sordello, V. Maurino, C. Minero, Improved photochemistry of TiO₂ inverse opals and some examples, in: D.S. Saha (Ed.), *Molecular Photochemistry – Various Aspects*, InTech, Rijeka, Croatia, 2012, pp. 63–86.
- [19] J.I.L. Chen, E. Loso, N. Ebrahim, G.A. Ozin, *J. Am. Chem. Soc.* 130 (2008) 5420–5421.
- [20] J.I.L. Chen, G. von Freymann, S.Y. Choi, V. Kitaev, G.A. Ozin, *Adv. Mater.* 18 (2006) 1915–1919.
- [21] F. Sordello, C. Duca, V. Maurino, C. Minero, *Chem. Commun.* 47 (2011) 6147–6149.
- [22] F. Sordello, V. Maurino, C. Minero, *J. Mater. Chem.* 21 (2011) 19144–19152.
- [23] M. Wu, J. Liu, J. Jin, C. Wang, S. Huang, Z. Deng, Y. Li, B.-L. Su, *Appl. Catal. B: Environ.* 150–151 (2014) 411–420.
- [24] F. Sun, W. Wang, L. Zhang, J. Xu, *Appl. Catal. B: Environ.* 125 (2012) 144–148.
- [25] D. Qi, L. Lu, Z. Xi, L. Wang, J. Zhang, *Appl. Catal. B: Environ.* 160–161 (2014) 621–628.
- [26] S. Chai, G. Zhao, Y. Wang, Y.-n. Zhang, Y. Wang, Y. Jin, X. Huang, *Appl. Catal. B: Environ.* 147 (2014) 275–286.
- [27] G.I.N. Waterhouse, M.R. Waterland, *Polyhedron* 26 (2007) 356–368.
- [28] J.W. Goodwin, J. Hearn, C.C. Ho, R.H. Ottewill, *Colloid Polym. Sci.* 252 (1974) 464–471.
- [29] H. Zhang, J.F. Banfield, *J. Phys. Chem. B* 104 (2000) 3481–3487.
- [30] S. Brunauer, P.H. Emmett, E. Teller, *J. Am. Chem. Soc.* 60 (1938) 309–319.
- [31] S.G. Johnson, J.D. Joannopoulos, *Opt. Express* 8 (2001) 173–190.
- [32] C.-T. Dinh, T.-D. Nguyen, F. Kleitz, T.-O. Do, *ACS Nano* 3 (2009) 3737–3743.
- [33] J. Joo, S.G. Kwon, T. Yu, M. Cho, J. Lee, J. Yoon, T. Hyeon, *J. Phys. Chem. B* 109 (2005) 15297–15302.
- [34] Y.-w. Jun, M.F. Casula, J.-H. Sim, S.Y. Kim, J. Cheon, A.P. Alivisatos, *J. Am. Chem. Soc.* 125 (2003) 15981–15985.
- [35] X.-L. Li, Q. Peng, J.-X. Yi, X. Wang, Y. Li, *Chem. Eur. J.* 12 (2006) 2383–2391.
- [36] B. Kraeutler, A.J. Bard, *J. Am. Chem. Soc.* 100 (1978) 4317–4318.
- [37] C. Minero, D. Vione, *Appl. Catal. B: Environ.* 67 (2006) 257–269.
- [38] G.E. Jellison, L.A. Boatner, J.D. Budai, B.S. Jeong, D.P. Norton, *J. Appl. Phys.* 93 (2003) 9537–9541.
- [39] W.Q. Fang, X.-Q. Gong, H.G. Yang, *J. Phys. Chem. Lett.* 2 (2011) 725–734.
- [40] H.J. Yun, H. Lee, J.B. Joo, N.D. Kim, J. Yi, *J. Nanosci. Nanotechnol.* 11 (2011) 1688–1691.
- [41] T. Kimijima, T. Sasaki, M. Nakaya, K. Kanie, A. Muramatsu, *Chem. Lett.* 39 (2010) 1080–1081.
- [42] L. Kavan, M. Grätzel, S.E. Gilbert, C. Klemenz, H.J. Scheel, *J. Am. Chem. Soc.* 118 (1996) 6716–6723.
- [43] Z. Kasarevic-Popovic, D. Behar, J. Rabani, *J. Phys. Chem. B* 108 (2004) 20291–20295.
- [44] R. Baba, S. Nakabayashi, A. Fujishima, K. Honda, *J. Phys. Chem.* 89 (1985) 1902–1905.
- [45] J. Yu, J. Low, W. Xiao, P. Zhou, M. Jaroniec, *J. Am. Chem. Soc.* 136 (2014) 8839–8842.
- [46] J. Yu, J. Fan, B. Cheng, *J. Power Sources* 196 (2011) 7891–7898.
- [47] C. Karunakaran, G. Abiramasundari, P. Gomathisankar, G. Manikandan, V. Anandi, *Mater. Res. Bull.* 46 (2011) 1586–1592.